7-15-2019

Distinct Patterns of Default Mode and Executive Control Network Circuitry Contribute to Present and Future Executive Function in Older Adults

Christopher A. Brown
University of Kentucky

Frederick A. Schmitt
University of Kentucky, fascom@uky.edu

Charles D. Smith
University of Kentucky, charles.smith.md@uky.edu

Brian T. Gold
University of Kentucky, brian.gold@uky.edu

Distinct Patterns of Default Mode and Executive Control Network Circuitry Contribute to Present and Future Executive Function in Older Adults

Digital Object Identifier (DOI)
https://doi.org/10.1016/j.neuroimage.2019.03.073

Notes/Citation Information
Published in *NeuroImage*, v. 195.

NeuroImage 195 (2019) 320–332

Contents lists available at ScienceDirect

NeuroImage

journal homepage: www.elsevier.com/locate/neuroimage

Distinct patterns of default mode and executive control network circuitry contribute to present and future executive function in older adults

Christopher A. Brown [a], Frederick A. Schmitt [b,c,d], Charles D. Smith [b,c,e], Brian T. Gold [a,b,e,*]

[a] Department of Neuroscience, University of Kentucky, Lexington, KY, 40536, USA
[b] Sanders-Brown Center on Aging, University of Kentucky, Lexington, KY, 40536, USA
[c] Department of Neurology, University of Kentucky, Lexington, KY, 40536, USA
[d] Department of Psychiatry, University of Kentucky, Lexington, KY, 40536, USA
[e] Magnetic Resonance Imaging and Spectroscopy Center, University of Kentucky, Lexington, KY, 40536, USA

A B S T R A C T

Executive function (EF) performance in older adults has been linked with functional and structural profiles within the executive control network (ECN) and default mode network (DMN), white matter hyperintensities (WMH) burden and levels of Alzheimer's disease (AD) pathology. Here, we simultaneously explored the unique contributions of these factors to baseline and longitudinal EF performance in older adults. Thirty-two cognitively normal (CN) older adults underwent neuropsychological testing at baseline and annually for three years. Neuroimaging and AD pathology measures were collected at baseline. Separate linear regression models were used to determine which of these variables predicted composite EF scores at baseline and/or average annual change in composite ΔEF scores over the three-year follow-up period. Results demonstrated that low DMN deactivation, high ECN activation and WMH burden were the main predictors of EF scores at baseline. In contrast, poor DMN and ECN WM microstructure and higher AD pathology predicted greater annual decline in EF scores. Subsequent mediation analysis demonstrated that DMN WM microstructure uniquely mediated the relationship between AD pathology and ΔEF. These results suggest that functional activation patterns within the DMN and ECN and WMHs contribute to baseline EF while structural connectivity within these networks impact longitudinal EF performance in older adults.

1. Introduction

Executive function (EF) describes the human capacity for flexible and adaptive thought processes, such as working memory, task switching, and inhibitory control (Miller and Cohen, 2001). Cognitively normal (CN) older adults show significant declines in EF compared to younger adults (Zelazo et al., 2004). Furthermore, decline in EF is associated with poorer quality of life and decreased functional independence in older adults (Bell-McGinty et al., 2002; Pathy et al., 2006). However, the mechanisms contributing to decreased EF in CN older adults are poorly understood. These mechanisms may include alterations in brain function and structure, accumulating white matter hyperintensities (WMH) and/or Alzheimer's disease (AD) pathology.

Much of the research seeking to identify functional mechanisms contributing to EF declines in older adults have focused on regions belonging to the executive-control network (ECN). The majority of studies have demonstrated that functional brain activity within portions of the ECN increase with age (Grady, 2012; Spreng et al., 2010). However, studies examining how these age-related increases in activity are associated with EF performance have been equivocal, with some finding no relationship (Grady, 2012) and others finding that increased activity is associated with poorer task performance (Stern, 2009; Zhu et al., 2015). This has led researchers to view this activity as either a sign of reduced efficiency (Stern, 2009; Zhu et al., 2015) or a failed attempt at compensation (Grady, 2012; Park and Reuter-Lorenz, 2009).

More recent research suggests that other networks may also play an important role in EF in older adults. In particular, the default mode network (DMN) may be an important contributor to EF performance in older adults. The DMN is a set of regions that are most active at rest and decrease in activity during externally-directed tasks. The DMN is thought to be primarily responsible for internally-focused thought processes, such as autobiographical memory and experience of the self, which must be decreased during externally-directed tasks (Andrews-Hanna et al., 2014; Buckner et al., 2005; Raichle et al., 2001). However, the ability to decrease activity in the DMN during tasks, termed deactivation, decreases linearly across the adult lifespan (Grady et al., 2006). Due to its role in autobiographical memory, much of the research examining the DMN's role in cognition has focused on memory (Buckner et al., 2005; Gould et al., 2006; Lustig et al., 2003; Vannini et al., 2012), while fewer have explored associations with EF. However, there is some evidence that age-related reduction in DMN deactivation is associated with poorer EF task performance (Brown et al., 2015; Persson et al., 2007).

* Corresponding author. Department of Neuroscience, College of Medicine, University of Kentucky, Lexington, KY, 40536, USA.
E-mail address: brian.gold@uky.edu (B.T. Gold).

https://doi.org/10.1016/j.neuroimage.2019.03.073
Received 13 December 2018; Received in revised form 16 February 2019; Accepted 30 March 2019
Available online 4 April 2019

In addition to functional activation patterns, alterations in ECN and DMN structural connectivity (i.e., white matter microstructure) may contribute to reduced EF in older adults. White matter (WM) microstructure refers to the organizational coherence and density of WM and can be assessed *in vivo* through the use of diffusion tensor imaging (DTI). Declines in microstructural properties of WM are consistently observed in aging and are thought to reflect decreased myelin and/or axonal density (Bartzokis et al., 2004; Beaulieu, 2002; Salat et al., 2005). Early work examining DTI and EF relationships primarily focused on frontal WM and fronto-parietal association tracts belonging to the ECN, such as the superior longitudinal fasciculus (Gold et al., 2010; Madden et al., 2004), but recent work has also demonstrated relationships between microstructure in WM pathways connecting DMN regions and EF performance (Brown et al., 2015).

Finally, EF performance in older adults may also be influenced by the accumulation of neuropathology. The most prevalent neuropathology in aging is AD pathology, which consists of amyloid plaques made up of β-amyloid (Aβ) and neurofibrillary tangles made up of tau (Glenner and Wong, 1984; Grundke-Iqbal et al., 1986). Importantly, AD pathology is present in approximately 30% of CN older adults over the age of 65, representing a prolonged preclinical disease stage during which pathology accumulates but no clinical signs are present (Morris et al., 1996; Price et al., 2009; Sperling et al., 2009). The most sensitive and specific marker of AD pathology is the CSF tau/$A\beta_{42}$ ratio (Shaw et al., 2009), and several studies have demonstrated that higher CSF tau/$A\beta_{42}$ ratios predict future decline (Fagan et al., 2007; Vos et al., 2013). While AD is typically thought of as primarily affecting memory in early disease stages, several studies have demonstrated poorer performance on tests of EF during preclinical disease stages (Albert et al., 2001; Almkvist, 1996; Blacker et al., 2007).

In addition to AD pathology, many older adults also harbor significant levels of cerebrovascular disease (CVD) pathology. The most commonly used *in vivo* marker of CVD pathology is the presence of WMH assessed using fluid attenuated inversion recovery (FLAIR) imaging (Breteler et al., 1994; COHEN et al., 2002). These areas of WMH correspond with areas of axonal and myelin loss post-mortem and often occur in areas with reduced vascular integrity and increased inflammatory infiltrate (Grafton et al., 1991; Young et al., 2008). WMHs are seen in approximately 90% of CN older adults aged 60–90 (de Leeuw, 2001) and have been associated with poorer EF during preclinical disease stages (COHEN et al., 2002; Debette and Markus, 2010).

It is relevant to note that the functional, structural, and pathological mechanisms described above frequently overlap, and, in fact, are themselves associated with each other. For example, previous studies have demonstrated associations between neuropathology and functional activity (Hedden et al., 2012; Oh et al., 2015; Sperling et al., 2009), between neuropathology and WM microstructure (Gold et al., 2014; Kantarci et al., 2014; Taylor et al., 2007), and between WM microstructure and functional activity (Brown et al., 2015; Daselaar et al., 2013; Zhu et al., 2015). Despite this fact, a majority studies examining how each of these measures impact EF in aging have focused on only functional, structural or pathological mechanisms.

In the present study, we sought to explore the relative contributions of both DMN and ECN functional and structural profiles and measures of neuropathology to EF in cognitively normal (CN) older adults. We first sought to explore how these measures associate with standardized neuropsychological measures cross-sectionally. Second, we examined how these DMN and ECN measures may predict longitudinal EF neuropsychological performance over-and-above effects of neuropathology. We hypothesized that both DMN and ECN function/structure would be associated with cross-sectional EF performance on standardized neuropsychological measures. Further, we predicted that baseline DMN and ECN function and/or structure may mediate the effects of neuropathology on change in EF neuropsychological performance over time.

2. Methods

2.1. Participants

Written informed consent was obtained from each participant under an approved University of Kentucky Institutional Review Board protocol. Thirty-two CN older adults (age at baseline: 66–93 years old) were selected from one of our previous neuroimaging studies (Brown et al., 2018) of 39 CN older adults (ages 65–93) based on availability of longitudinal neuropsychological testing and quality baseline neuroimaging data. The original cohort was recruited from a larger cohort of CN older adults followed by the University of Kentucky Sanders-Brown Center on Aging (SBCoA), which has been described previously (Schmitt et al., 2012). Exclusion criteria for all participants were significant head injury (operationally defined as loss of consciousness for greater than five minutes), heart disease, psychiatric or neurological disorder, claustrophobia, pacemakers, or presence of metal fragments and/or metallic implants contraindicated for MRI. Seven participants from the original cohort were excluded from the current study due to: poor neuroimaging data quality ($n = 4$, see (Brown et al., 2018) for details), decision not to enroll in neuropsychological testing portion of the study ($n = 2$) or loss to follow-up after baseline visit ($n = 1$). Neuropsychological data was available for 32 participants at baseline and this data was used in the cross-sectional analyses. Neuropsychological data was available for 31 participants at one-year follow-up, for 29 participants at two-year follow-up, and 28 participants at three-year follow-up. The average number of annual visits (including baseline) available per participant was 3.75 ± 0.51 (range = 2–4, median = 4). Three individuals were identified as outliers in average ΔEF score (>3 SD from mean) and were not included in the regression analyses. Therefore, a total of 29 participants were included in longitudinal analyses. Baseline demographics and mean outcome measures are reported for the initial group of 32 participants and the subgroup of 29 participants used in longitudinal analyses in Table 1 (all values represent baseline data except for the average annual change in EF). At baseline, 7/32 participants were $A\beta_{42}$ +, of which 4/7 participants were tau/$A\beta_{42}$ + based on established thresholds.

2.2. Evaluation of EF

All participants underwent the standard battery of neuropsychological tests included in the UDS-2 at baseline. Individuals returned annually to undergo the UDS battery (Weintraub et al., 2002). At follow-up testing sessions, participants completed the UDS-3. The UDS-2 and UDS-3 are

Table 1
Demographic and outcome measures.

	Baseline Group (n = 32)	Longitudinal Subgroup (n = 29)
Age	77.7 (6.57)	77.8 (6.82)
Sex (M:F)	14:18	13:16
Education	16.5 (2.41)	16.7 (2.44)
DMN-naWM FA	0.58 (0.026)	0.58 (0.027)
DMN Deactivation Magnitude (% signal change)	0.10 (0.119)	0.11 (0.109)
ECN-naWM FA	0.57 (0.028)	0.57 (0.029)
ECN Activation Magnitude (% signal change)	0.20 (0.212)	0.18 (0.215)
CSF $A\beta_{42}$ (pg/mL)	271.4 (79.21)	270.2 (79.11)
CSF Tau (pg/mL)	56.9 (16.29)	57.2 (16.75)
CSF Tau/$A\beta_{42}$	0.24 (0.140)	0.24 (0.142)
WMH Volume/ICV	0.011 (0.007)	0.011 (.007)
MMSE*	30 (27–30)	30 (27–30)
CDR-SB*	0 (0–0)	0 (0–0)
Baseline EF Composite	−0.12 (0.907)	0.08 (0.621)
Average Annual ΔEF	–	−0.04 (0.228)

Mean (S.D.) for individuals included in baseline analyses (left) and longitudinal analyses (right). All measures reflect values at baseline except for the Average Annual ΔEF. *Median (range) are provided for MMSE and CDR-SB scores.

not identical. Thus, EF-related tests common to the UDS-2 and UDS-3 were selected for use in the present study: Trailmaking Part A (TM-A), Trailmaking Part B (TM-B), and the Digit Symbol test from the Wechsler Adult Intelligence Scale-IV (WAIS-DS). Raw scores were first standardized based on age, sex, and education using scores generated from the larger SBCoA cohort, as previously described (Kryscio et al., 2016). Age, sex, and education-standardized scores for TM-A were then regressed out of TM-B and WAIS-DS standardized scores in order to exclude components of raw processing and motor speed common to all tests (Salthouse, 2011). The resulting residuals were then combined to form a composite EF score by subtracting the TM-B residuals (higher scores = worse performance) from the WAIS-DS residuals (higher scores = better performance) and dividing by 2. Therefore, higher EF composite scores reflected better performance.

The EF composite was calculated for each participant at each visit. One-year change between each visit was calculated by subtracting the EF score of the current visit from the previous visit (i.e. EF composite at Year 1 visit – EF composite at baseline visit). Our study focused on average annual EF change rates. Thus, each participant's *average* annual change in EF was calculated by averaging all of that individual's available one-year change scores (average the change from year 0 to year 1, year 1 to year 2, and year 2 to year 3).

2.3. CSF sampling and analysis

Lumbar puncture was performed following an overnight fast, as previously described (Gold et al., 2014). Samples were shipped on dry ice to the Biomarker Research Laboratory at the University of Pennsylvania Medical Center, where the xMAP Luminex Platform (Luminex Corp, Austin TX) with Innogenetics (INNO-BIA, AlzBio3; Ghent, Belgium) immunoassay kit was used to measure CSF concentrations of $A\beta_{42}$ and total tau as previously described (Shaw et al., 2009). The CSF tau/$A\beta_{42}$ was then calculated and used in analyses due to its high sensitivity and specificity for AD pathology (Shaw et al., 2009). The CSF tau/$A\beta_{42}$ ratios were log-transformed before statistical analyses due to their skewed distribution.

2.4. fMRI paradigm

Participants performed a visual working memory paradigm during fMRI scanning. The paradigm was a modified delayed-match-to-sample task with multiple targets and repeating intervening distractors, which increases demands on executive processes (Jiang, 2000; Kane and Engle, 2002). The task paradigm has been described in detail previously (Brown et al., 2018; Gold et al., 2017). Briefly, participants were asked to 'hold in mind' two target images and indicate whether or not each of 12 serially presented sample images represented a match with either target image. These sample images were one of four repeating images that were either one of the two target images or one of two repeating distractor images. Each fMRI run consisted of 8 working memory task blocks (28s each) and 9 visual baseline blocks (10s each), which occurred between task blocks and at the start and end of each run. Participants performed two fMRI runs. Relationships between fMRI activation/deactivation patterns and working memory task performance in the present participants have been reported previously (Brown et al., 2018; Gold et al., 2017). In the present study, we focused on the relationships between activation/deactivation magnitudes and neuropsychological performance.

2.5. Image acquisition

All images were collected using a Siemens Trio TIM 3 Tesla scanner with a 32-channel head coil at the University of Kentucky Magnetic Resonance Imaging and Spectroscopy Center (MRISC). The protocol consisted of the following sequences collected in the order in which they are listed: 1) High-resolution T1-weighted anatomical image, 2) Two task-fMRI blood-oxygen level dependent (BOLD) T2*-weighted functional imaging runs, 3) one resting state (rs)-fMRI BOLD T2*-weighted functional imaging run, 4) diffusion tensor imaging (DTI), 5) fluid-attenuated inversion recovery (FLAIR) imaging.

The high-resolution T1-weighted image was acquired using magnetization-prepared rapid echo gradient-echo (MPRAGE) sequence [Repetition time (TR) = 2530 ms, Echo time (TE) = 2.26 ms, inversion time (TI) = 1100 ms, Flip angle = 7°, acquisition matrix = 256 × 256 × 176, field of view (FOV) = 256 × 256 mm, 1 mm isotropic voxels]. Task- and rs-fMRI were acquired using gradient-echo echo-planar imaging (EPI) [TR = 2000 ms, TE = 27 ms, Flip angle = 83°, acquisition matrix = 64 × 64, FOV = 243 × 243 mm, 3.8 mm isotropic voxels, 36 interleaved slices]. DTI was acquired using a double-spin echo EPI sequence [TR = 8000 ms, TE = 96 ms, Flip angle = 90°, FOV = 224 × 224 mm, 2 mm isotropic voxels, 52 contiguous slices] with 60 non-collinear encoding directions ($b = 1000$ s/mm^2) plus 8 images without diffusion weighting (b0). FLAIR images were collected using a fat-saturated, turbo-spin echo (TSE) sequence [TR = 9000 ms, TE = 89 ms, TI = 2500 ms, Flip Angle = 90°, Refocusing Angle = 130°, acquisition matrix = 256 × 174 × 34, 1 × 1 × 4 mm voxels].

2.6. Functional imaging analysis

Analyses focused on participant's mean functional activation/deactivation magnitude within two network templates: the DMN and ECN. The templates were developed in our previous studies that involved both younger and older adults (Brown et al., 2018; Gold et al., 2017). These templates were utilized instead of using a standard rs-fMRI template, such as Stanford rs-fMRI atlases, as they incorporate data from older adults, and are thus more appropriate for the study of older adults. The template development has been described in full detail elsewhere (Brown et al., 2018). Briefly, the functional templates were developed using the following steps. The FMRIB software library (FSL) version 5.0.9 (Jenkinson et al., 2012; Smith et al., 2004) was used for pre-processing and analysis of neuroimaging data. Following motion correction and non-linear registration to the MNI152 T1 2 mm^3, both task- and rs-fMRI data were scrubbed for motion with both regression of motion parameters and removal of motion outliers using a frame-wise displacement threshold of >0.5 mm (Power et al., 2012). Further nuisance regression removed signal of white matter and CSF (Brown et al., 2018). The residuals from these pre-processing steps were then used for time-series analyses.

The templates were formed by performing independent component analysis separately for each task- and rs-fMRI run, averaging DMN/ECN components from task-based runs, and masking them with the DMN/ECN component from rs-fMRI in order to include regions showing activation/deactivation during the task and connectivity at rest (Brown et al., 2018). Using this approach, only regions showing task-related activity that were part of the canonical resting-state networks were included our final templates (Fig. 1). Subsequent analyses focused on BOLD magnitude within the functional templates. These functional templates are available for use and can be downloaded from our lab website (https://sites.google.com/site/btgoldlaboratory/, also available at http://doi.org/10.13140/RG.2.2.34709.78567).

Time-series were extracted from the functional templates (Fig. 1). BOLD signal during baseline was computed by averaging the middle 6s of all baseline blocks (in order to avoid the upshoot and downshoot associated with the onset/offset of blocks). BOLD signal during the task was computed by averaging the middle 6s of all working memory blocks (to parallel sampling of baseline blocks). Activation/deactivation within the functional templates was then computed as percent signal change by subtracting the BOLD signal during the baseline from BOLD signal during the task and multiplying by 100. For ease of interpretation, deactivation magnitude within the functional DMN template is reported by inverting the sign of % signal change (i.e. more negative % signal change is represented as more positive deactivation magnitude).

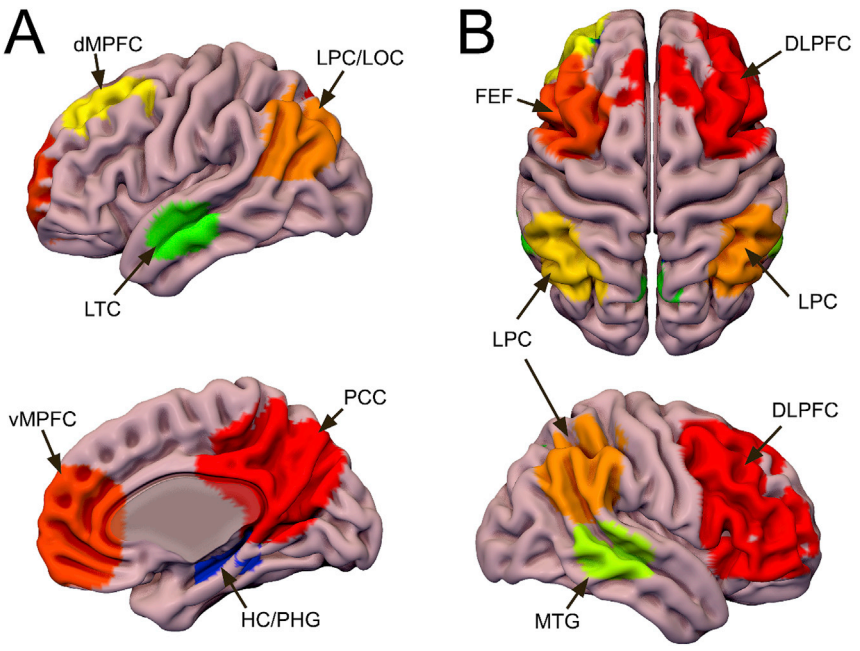

Fig. 1. DMN and ECN Functional Templates. DMN and ECN regions identified using ICA on both task- and rs-fMRI. The task-fMRI components were masked by the corresponding rs-fMRI components to create a template of regions showing activation/deactivation during the task and connectivity at rest. **A:** The DMN functional template includes the posterior cingulate cortex/precuneus (PCC/pC), ventromedial prefrontal cortex (vMPFC), dorsomedial prefrontal cortex (dMPFC), lateral temporal cortices (LTC), lateral parietal/occipital cortices (LPC/LOC), and portions of the hippocampus and parahippocampal gyrus (HC/PHG). **B:** The ECN functional template includes bilateral dorsolateral prefrontal cortex (DLPFC), frontal eye fields (FEF), lateral parietal cortices (LPC), and middle temporal gyri (MTG). **Both:** These regions were used to extract time-series for functional analyses and as seeds for probabilistic tractography. Surf Ice (https://www.nitrc.org/projects/surfice/) was used to create this display of the DMN template on the surface of the MNI152 T1 brain.

2.7. FLAIR analysis

FLAIR images were used to measure WMH volume and aid the development of a DTI-based microstructural templates within normal appearing white matter (naWM) with the same participants (Brown et al., 2018). A semi-automated process was used to identify WMH as previously described (Gold et al., 2017; Smith et al., 2016). Briefly, T1 structural images and FLAIR images were both corrected for inhomogeneities using the N3 correction in MIPAV (http://mipav.cit.nih.gov), and T1 images were then segmented using FreeSurfer (Dale et al., 1999; Fischl et al., 2002) to create a WM template. The resulting WM template was linearly registered to the FLAIR image using FLIRT, then dilated once in 2.5 days using MIPAV, and finally underwent a 1 mm Gaussian blur using FSL's SUSAN. The resulting mask was then applied to the FLAIR image, and a histogram of voxel-intensities for the FLAIR-WM image was generated. After applying a two-Gaussian model in order to identify the mean and standard deviation of the dominant fit, the FLAIR-WM image was thresholded to include only voxels >2.33 SD above this mean to form a WMH mask. This mask was manually edited to remove artefactual voxels in regions between lateral ventricles and in inferior slices (Smith et al., 2016). WMH volume was then calculated using fslstats and normalized to intracranial volume (ICV). Normalized WMH volumes were log-transformed prior to inclusion in statistical analyses.

The WMH mask was further used in the creation of DTI-based microstructural templates within naWM. Specifically, the WMH mask was registered to the average b0 image from DTI to restrict subsequent DTI analyses (described in section 2.8) to regions of naWM. The TBSS non-FA pipeline was used to register WMH masks in diffusion space to the FMRIB58 1 mm template (Smith et al., 2006), which were then used to determine naWM for each participant (described in section 2.8).

2.8. DTI analysis

Analyses focused on participant's mean FA values within DMN and ECN naWM templates developed using data from our previous study that included both younger and older adults. Mean FA was selected as it provides a summary measure of overall WM organization and is the most common DTI metric used for correlations with cognition in the literature. Mean diffusivity was not analyzed in this study as it is strongly negatively correlated with FA. The DTI analysis procedures used to develop the WM templates is described in detail elsewhere (Brown et al., 2018). Previous work from our laboratory has shown that including data from both younger and older adults in development of white matter templates provides a more accurate template for use in aging populations than using data from younger or older adults only (Brown et al., 2017). In order to allow for easier reproducibility of these data, all templates used in this study have been made available on publicly accessible websites (https://sites.google.com/site/btgoldlaboratory/ and http://doi.org/10.13140/RG.2.2.34709.78567). Briefly, the WM templates were developed using the following steps. The templates were generated from individual tractography results in our previous study after data had undergone the standard pre-processing described below.

Tractography was performed using BEDPOSTX and PROBTRACKX2 in network mode with the regions identified in each functional template (DMN or ECN) as seed regions (Behrens et al., 2007). Successful streamlines were those that started in one seed region from the functional template and ended in another seed region from the functional template without violating standard curvature, distance, and FA thresholds. Individual tractography results were corrected for total streamlines attempted and waytotal, registered to standard space using transformations from tract-based spatial statistics (TBSS), and then averaged and thresholded to form group templates of DMN and ECN WM pathways.

FMRIB's Diffusion Toolbox (FDT) v.3.0 was used for processing and analyses as previously described (Brown et al., 2018). Initial pre-processing included use of EDDY for motion and eddy-current correction with automatic replacement of outliers (Andersson et al., 2016; Andersson and Sotiropoulos, 2016), brain extraction using the average b0 image, and generation of a voxel-wise tensor model using DTIFIT. The voxel-wise tensor model was used to generate an FA image, which was then registered to the FMRIB58 FA 1 mm template using the tract-based spatial statistics (TBSS) pipeline (Smith et al., 2006). A group skeleton was formed using a threshold of FA > 0.2 and individual participant data was projected onto this skeleton in order to minimize partial volume effects and correct for residual misalignments. The group templates were then masked by the mean FA skeleton to form skeletonized WM templates. FA was then measured within individualized DMN-naWM and ECN-naWM masks. These individualized naWM masks were formed by masking the group skeleton templates by each participant's WMH image in FMRIB58 1 mm space (described above) and

including only voxels that were not part of the WMHs (i.e. naWM). The average FA within each participant's DMN-naWM and ECN-naWM skeleton masks was then calculated using fslstats.

2.9. Statistical analyses

SPSS 24 (IBM, Chicago, IL) was used for all statistical analyses. Cross-sectional relationships between potential correlates of EF were first explored using bivariate correlations between our independent variables: DMN deactivation, FA in DMN-naWM, ECN activation, FA in ECN-naWM, WMH volume, and CSF tau/Aβ_{42} ratio. Multiple linear regression was then used to explore the relationship between these predictors and baseline EF with a backward selection step to identify only the significant predictors (elimination criteria of $p > .10$). Due to high co-linearity between FA in DMN-naWM and ECN-naWM, regressions were initially run separately for each network. In cases where multiple measures remained in the final model, mediation models were used to explore how these measures contribute to baseline EF.

Longitudinal analyses examined whether any neuroimaging or neuropathology measures could predict average annual change in EF (ΔEF) scores after controlling for baseline EF scores. Similar to baseline analyses, multiple linear regression analyses were performed separately for each network (DMN or ECN) with a backward selection step to identify only the significant predictors (elimination criteria of $p > .10$). In cases where multiple measures remained in the final model, mediation models were used to explore how these measures contribute to ΔEF scores.

Due to the presence of multivariate relationships, Preacher and Hayes mediation analyses (Hayes, 2013) were used to determine if any variables mediated the relationships between another variable and EF scores. This analysis seeks to examine whether the total effect (c) of some predictor (X) on the outcome measure (Y) is due to a significant direct effect (c') of X on Y or instead is explained by an indirect effect (ab) of X on Y through a mediator variable (M). Significance was tested using 5000 bootstrap samples to calculate bias-corrected 95% confidence intervals. Indirect effects with bootstrapped 95% confidence intervals not crossing 0 were considered significant.

2.10. Supplemental analysis

A supplementary analysis utilized linear mixed modeling rather than the average yearly change in EF to evaluate the impact of each baseline measure on longitudinal change in EF. In these analyses, time was used as a continuous variable in years with the baseline visit as year 0. Additional predictors included FA in DMN-naWM, FA in ECN-naWM, DMN deactivation magnitude, ECN activation magnitude, WMH volume and CSF tau/Aβ_{42}. Both main effects and the time × predictor interaction were assessed for each model. For all models, REML was used for estimation and a compound symmetry variance structure was used for repeated effects. As six separate primary models were run, those interactions with $p < .05/6 = 0.0083$ were considered significant. A final model was run using those predictors found to have a significant predictor × time interaction in the primary models.

3. Results

3.1. Functional and WM templates

The DMN and ECN functional templates created from data from our previous study with younger and older adults (Brown et al., 2018) are shown in Fig. 1. The functional DMN template includes bilateral medial prefrontal, posterior cingulate, dorsomedial prefrontal, lateral parietal/occipital, and lateral parietal cortices, as well as the left parahippocampal gyrus and right hippocampus (Fig. 1a). The ECN template includes portions of the dorsolateral prefrontal cortex, dorsal parietal cortices, and lateral temporal cortices (Fig. 1b). The DMN regions are consistent with those described as canonical DMN regions (Buckner et al., 2005), while the ECN regions are most consistent with the superordinate cognitive control network (Cole and Schneider, 2007; Niendam et al., 2012).

The structural DMN and ECN WM templates are shown in Fig. 2. The DMN-WM template consists of WM pathways connecting DMN functional regions (i.e. deactivations) within the same participants including portions of the cingulum, superior longitudinal fasciculus, inferior longitudinal fasciculus, fornix, corpus callosum genu, and corpus callosum splenium. The ECN template consists of WM pathways connecting ECN functional regions (i.e. activations) within the same participants including portions of the superior longitudinal fasciculus, corpus callosum genu, corpus callosum splenium, and inferior fronto-occipital fasciculus.

3.2. Baseline relationships

There was a strong correlation between both accuracy ($r = 0.43$, $p = .014$) and reaction time ($r = -0.54$, $p = .001$) on the fMRI task used to generate the functional templates and baseline EF scores in the present sample. At baseline, many of the neuroimaging and neuropathology measures were correlated (Table 2). Results of multiple linear regression indicated that baseline EF was predicted by the full DMN model ($F_{4,27} = 3.83$, $p = .014$). In this model, DMN deactivation was the only significant predictor ($\beta = 0.45$, $t = 2.55$, $p = .012$), while FA in DMN-naWM ($\beta = 0.09$, $t = 0.53$, $p = .602$), CSF tau/Aβ_{42} ($\beta = 0.129$, $t = 0.74$, $p = .465$), and WMH volume ($\beta = -0.32$, $t = -1.99$, $p = .057$) were not significant predictors. The first step of backward selection ($F_{3,28} = 5.15$, $p = .006$) removed FA in DMN-naWM, and the final step removed CSF tau/Aβ_{42}, leaving both DMN deactivation ($\beta = 0.43$, $t = 2.84$, $p = .008$) and WMH volume ($\beta = -0.35$, $t = -2.33$, $p = .027$) as predictors in the final model ($F_{2,29} = 7.68$, $p = .002$) (Fig. 3a). Similarly, results indicated that baseline EF was also predicted by the full ECN model ($F_{4,27} = 2.90$, $p = .040$). In this model, ECN activation approached significance ($\beta = -0.38$, $t = -2.03$, $p = .052$), while FA in ECN-WM ($\beta = 0.06$, $t = 0.33$, $p = .742$), CSF tau/Aβ_{42} ($\beta = 0.094$, $t = 0.52$, $p = .609$), and WMH volume ($\beta = -0.31$, $t = -1.85$, $p = .075$) were not significant predictors. The first step of backward selection ($F_{3,28} = 3.96$, $p = .018$) removed FA in ECN-WM, and the final step removed CSF tau/Aβ_{42}, leaving both ECN activation ($\beta = -0.365$, $t = -2.29$, $p = .030$) and WMH volume ($\beta = -0.33$, $t = -2.08$, $p = .047$) as predictors in the final model ($F_{2,29} = 5.92$, $p = .007$) (Fig. 3b).

Several mediation models were then run to explore the potential mediation effects. The first model explored whether DMN deactivation and/or ECN activation mediated the effect of WMH volume on EF (Fig. 4a). Results of this model demonstrated that neither the combined ($ab = -0.08$ [-0.33, 0.03]) or individual indirect effects of ECN activation ($ab = -0.04$ [-0.35, 0.03]) and DMN deactivation ($ab = -0.04$ [-0.16, 0.01]) mediated the significant direct effect ($c' = -0.32$ [-0.63, −0.01]) of WMH volume on baseline EF. The second model explored whether DMN deactivation and/or WMH volume mediated the relationship between ECN activation and EF (Fig. 4b). Results demonstrated that the combined indirect effect of DMN deactivation and WMH volume ($ab = -0.23$ [-0.66, −0.002]) mediated the relationship between ECN activation and EF ($c' = -0.21$ [-0.56, 0.15]), but neither the individual indirect effect of WMH volume ($ab = -0.07$ [-0.23, 0.007]) nor of DMN deactivation ($ab = -0.16$ [-0.58, 0.009]) was significant. The final model explored whether ECN activation and/or WMH volume mediated the relationship between DMN deactivation and EF (Fig. 4c). Results demonstrated that while neither the combined indirect effect ($ab = 0.14$ [-0.002, 0.42] nor the indirect effect of WMH volume ($ab = 0.04$ [-0.05, 0.20] mediated the relationship between DMN deactivation and EF, the indirect effect of ECN activation ($ab = 0.099$ [0.001, 0.322]) did significantly mediate this relationship ($c' = 0.33$ [-0.02, 0.68]).

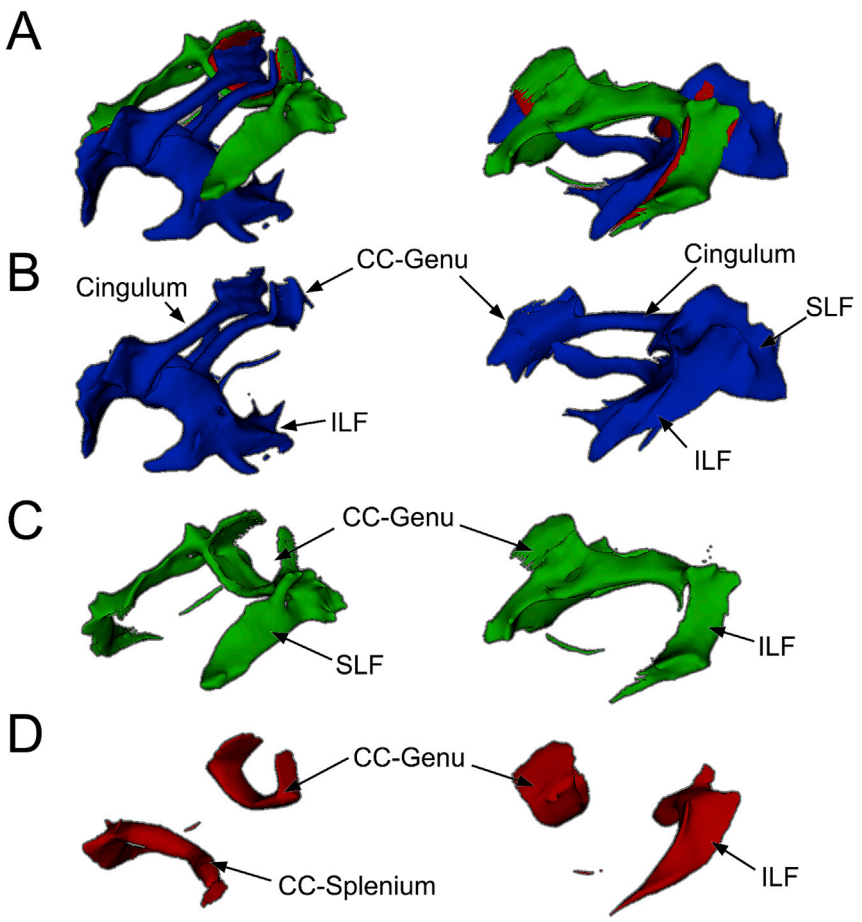

Fig. 2. DMN and ECN WM Templates. A: WM pathways connecting the DMN (blue) and ECN (green) with areas connecting both shown in red. **B:** WM pathways unique to the DMN include portions of the corpus callosum (CC) splenium and genu, cingulum, superior longitudinal fasciculus (SLF), and inferior longitudinal fasciculus (ILF). **C:** WM pathways unique to the ECN include portions of the SLF, CC-genu, and ILF. **D:** WM pathways that connected both DMN and ECN regions included portions of the CC genu and splenium and ILF. **A-D:** WM pathways were identified using probabilistic tractography and averaging individual results to form a single group template. The regions identified in the functional templates (Fig. 1) were used as seeds for tractography. Superior-lateral view on left and lateral view on right.

Table 2
Baseline relationships between imaging and CSF measures.

	DMN Deactivation magnitude	FA in DMN-naWM	ECN Activation Magnitude	FA in ECN-naWM	WMH Volume	CSF tau/$A\beta_{42}$
DMN Deactivation magnitude	–	**0.40 (.025)**	**−0.48 (.005)**	0.33 (.062)	−0.13 (.494)	**−0.39 (.029)**
FA in DMN-naWM		–	**−0.38 (.032)**	**0.91 (.000)**	−0.26 (.152)	**−0.35 (.047)**
ECN Activation Magnitude			–	**−0.40 (.022)**	0.20 (.262)	**0.39 (.026)**
FA in ECN-naWM				–	−0.22 (.231)	−0.32 (.071)
WMH Volume					–	−0.04 (.827)
CSF tau/$A\beta_{42}$						–

Values are Pearson-r with p-values in parentheses. Significant ($p < .05$) relationships are shown in bold. All analyses had $n = 32$.

3.3. Predicting longitudinal change in EF scores

All participants remained cognitively normal at follow-up with MMSE >27 and CDR-SB = 0 at all time points. EF declined -0.04 ± 0.228 units annually over the 3-year follow-up period. Higher baseline EF scores were associated with more negative ΔEF scores ($r = -0.46$, $p = .011$). Separate linear regression analyses were performed for the DMN and ECN to determine whether imaging and neuropathology measures could predict ΔEF scores after controlling for baseline EF. Results indicated that ΔEF scores were predicted by the full DMN model ($F_{5,23} = 6.61$, $p = .001$) after first entering baseline EF into the model ($F\text{-}change_{4,23} = 5.24$, $p = .004$). In this model, the only significant predictor other than baseline EF was FA in DMN-naWM ($\beta = 0.38$, $t = 2.35$, $p = .027$), while DMN deactivation ($\beta = 0.14$, $t = 0.99$, $p = .385$), CSF tau/$A\beta_{42}$ ($\beta = -0.23$, $t = -1.45$, $p = .161$), and WMH volume ($\beta = -0.15$, $t = -1.02$, $p = .320$) all failed to reach significance. The first step of backward selection ($F_{4,24} = 6.61$, $p < .001$) removed DMN deactivation, and the final step removed WMH volume, leaving both FA in DMN-naWM ($\beta = 0.44$, $t = 2.80$, $p = .010$) and CSF tau/$A\beta_{42}$ ($\beta = -0.26$, $t = -1.75$, $p = .093$) as predictors in the final model ($F_{3,25} = 10.59$, $p < .001$) (Fig. 5a). Similarly, results indicated that ΔEF scores were predicted by the full ECN model ($F_{5,23} = 7.01$, $p < .001$) after first entering baseline EF into the model ($F\text{-}change_{4,23} = 5.63$, $p = .003$). In this model, both FA in ECN-naWM ($\beta = 0.41$, $t = 2.71$, $p = .013$), CSF tau/$A\beta_{42}$ ($\beta = -0.41$, $t = -2.63$, $p = .015$) were significant, while neither ECN activation ($\beta = 0.23$, $t = 1.46$, $p = .159$) nor WMH volume ($\beta = -0.17$, $t = -1.18$, $p = .249$) were significant predictors. The first step of backward selection ($F_{4,24} = 8.28$, $p < .001$) removed WMH volume, and the final step removed ECN activation, leaving both FA in ECN-WM ($\beta = 0.39$, $t = 2.60$, $p = .016$) and CSF tau/$A\beta_{42}$ ($\beta = -0.31$, $t = -2.08$, $p = .048$) as predictors in the final model ($F_{3,25} = 9.96$, $p < .001$) (Fig. 5b).

As FA in DMN-WM and FA in ECN-WM were highly correlated, mediation models were run with only one of the variables entered at a time. Therefore, 4 mediation models were run: 1) CSF tau/$A\beta_{42}$ as a mediator of the FA in DMN-naWM and ΔEF score relationship, 2) CSF tau/$A\beta_{42}$ as a mediator of the FA in ECN-naWM and ΔEF score relationship, 3) FA in DMN-naWM as a mediator of the CSF tau/$A\beta_{42}$-and ΔEF score relationship, and 4) FA in ECN-naWM as a mediator of the CSF

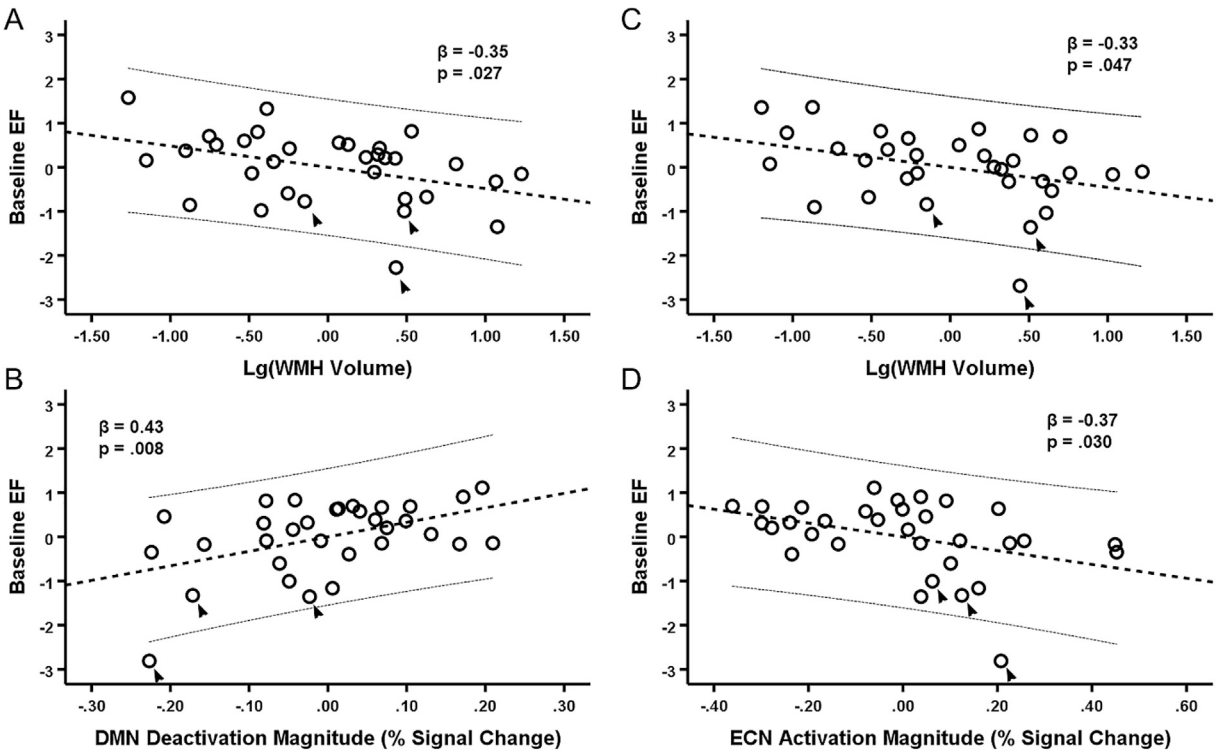

Fig. 3. Prediction of EF at Baseline by WMH volume, DMN deactivation, and ECN activation. A-B: Partial regression plots of baseline EF against WMH volume **(A)** and DMN deactivation **(B)** simultaneously. **C-D:** Partial regression plots of EF against WMH volume **(C)** and ECN activation **(D)** simultaneously. **A-D:** All values are mean-centered. The thick dashed line represents the linear best-fit and thin dashed lines are the 95% confidence interval for the predicted response. Includes all baseline participants (n = 32). The three participants not included in the longitudinal analyses are indicated by arrows.

tau/Aβ_{42} and ΔEF score relationship. In all models, baseline EF was used as a covariate on ΔEF scores. Results of the first two mediation analyses (Fig. 6c and d) found that CSF tau/Aβ_{42} did not mediate the effect of FA in DMN-naWM (c' = 0.44 [0.11, 0.76], ab = 0.11 [-0.01, 0.35]), nor did it mediate the effect of FA in ECN-naWM (c' = 0.39 [0.08, 0.71], ab = 0.11 [-0.02, 0.41]) on ΔEF scores. Results of the third model (Fig. 6a) demonstrated that FA in DMN-naWM fully mediated the relationship between CSF tau/Aβ_{42} and ΔEF scores (ab = −0.19 [-0.53, −0.01], c' = −0.26 [-0.57, 0.047]). Finally, the results of the fourth model (Fig. 6b) demonstrated that FA in ECN-WM partially mediated (ab = −0.15 [-0.405, −0.01]) the significant effect of CSF tau/Aβ_{42} on ΔEF scores (c' = −0.30 [-0.61, −0.002]).

3.4. Linear mixed modeling

Linear-mixed models were used to assess how baseline measures predicted the change in EF over time. For each model, time was input as a continuous variable in years, with the baseline visit as year 0. DMN deactivation magnitude, FA in DMN-naWM, ECN activation magnitude, FA in ECN-naWM, WMH volume, and CSF tau/Aβ_{42} were entered in separate models as main effects, along with a time × baseline predictor interaction. Results of these models are shown in Table 3 and found that the only two predictors with a significant interaction with time were FA in DMN-naWM and FA in ECN-naWM. An additional model was run using both FA in DMN-naWM and FA in ECN-naWM along with their interactions with time, but no predictor other than time was significant (Table 4). A final full model was run using the addition of FA in DMN-naWM × FA in ECN-naWM and FA in DMN-naWM × FA in ECN-naWM × time interactions. Results are provided in Table 4 and demonstrated significant FA in DMN-naWM × time, FA in ECN-naWM × time, and FA in DMN-naWM × FA in ECN-naWM × time interactions.

4. Discussion

We explored the relative contributions of functional and structural brain profiles, WMH burden and AD pathology to baseline and longitudinal EF performance in older adults. Results indicated that baseline EF was best predicted by ECN activation and DMN deactivation magnitudes and WMH volume. In contrast, ΔEF was predicted by DMN-WM and ECN-WM microstructure and AD pathological markers. However, DMN WM microstructure mediated the relationship between AD pathology and ΔEF. Together, our findings suggest that WMH volume and DMN/ECN functional patterns contribute to current EF performance of older adults, while measures of DMN and ECN WM microstructure appear to be better predictors of their future EF performance.

4.1. Baseline EF is associated with WMH volume, ECN activation, and DMN deactivation

In the present study, WMH volume, ECN activation, and DMN deactivation magnitude predicted baseline EF performance. These findings are consistent with separate studies which have demonstrated that greater WMH volume (COHEN et al., 2002; Debette and Markus, 2010), higher ECN activity (Rypma et al., 2006; Stern, 2009; Zhu et al., 2015), and less DMN deactivation (Brown et al., 2015; Persson et al., 2007; Prakash et al., 2012) are all associated with poorer performance during tasks placing high demands on EF in older adults. This study extends findings in previous studies concerning ECN and DMN activity to more broadly used clinical measures of EF (as has been shown with previous studies concerning WMHs). Further, the composite measure of EF utilized in the present study provides a global estimate of EF that is less tied to potentially idiosyncratic single measure results (Crane et al., 2008).

Moreover, our results from multivariate analyses suggest, that among a number of potential predictors, functional activation in the ECN,

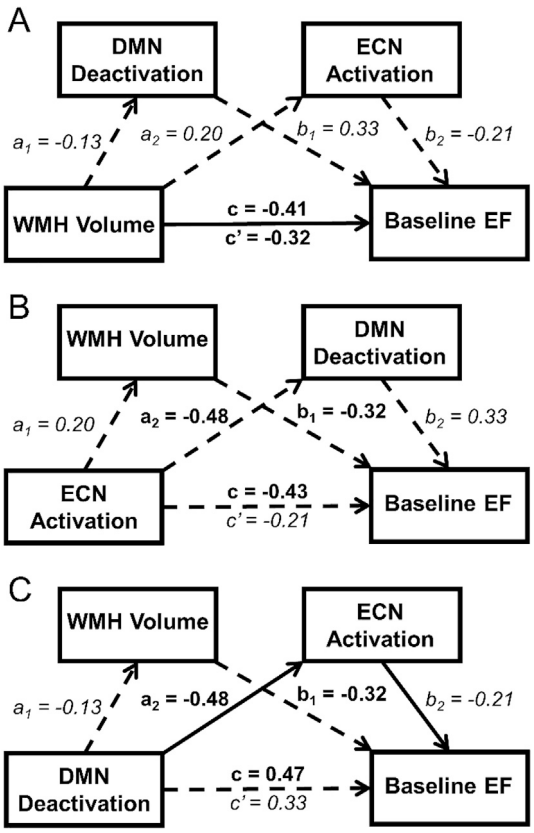

Fig. 4. Results of mediation models for baseline EF. A-C: Results of Preacher and Hayes mediation analyses with significant direct or indirect effects indicated by solid arrows and non-significant direct or indirect effects shown by dashed arrows. Standardized β-coefficients are shown next to the corresponding path with significant effects shown in bold and non-significant effects in italics. For all models, the total effect of X on Y (c) is shown above the horizontal arrow, while the direct effect of X on Y (c') after accounting for indirect effects is shown below the horizontal arrow. **A:** Results indicated that the indirect effects of DMN deactivation and ECN activation did not mediate the significant direct effect of WMH volume on baseline EF. **B:** Results indicated that the effect of ECN activation on baseline EF was mediated by the total indirect effects of DMN deactivation and WMH volume, but not by either individual indirect effect. **C:** Results indicated that the effect of DMN deactivation on baseline EF was mediated by the indirect effect of ECN activation but not of WMH volume.

deactivation in the DMN and WMH burden contributed to baseline EF performance in older adults. The finding that the association between ECN activation and EF was mediated by the indirect effects of WMH volume and DMN deactivation suggests that increased ECN activity may represent a compensatory response to greater levels of structural lesions in the form of WMHs and greater levels of ongoing activity in the DMN during the task. Notably, ECN activation was negatively correlated with EF performance. Therefore, increased ECN activity may represent a failed attempt at compensation and/or a sign of reduced efficiency (Barulli and Stern, 2013; Zhu et al., 2015).

In addition, greater levels of ongoing activity in the DMN during the task would be expected to negatively affect EF performance because it would result in greater ongoing internally-focused processes (Brown et al., 2015; Persson et al., 2007). Therefore, greater EF resources may be needed to suppress interference from ongoing DMN processes, possibly leaving fewer EF resources to devote to the task-at-hand. In contrast, those who successfully deactivate the DMN appear to be able to "free-up" neural resources for use in EF processes required by the task-at-hand.

As noted, WMH volume was also a significant predictor of baseline EF performance. This suggests that other factors outside of the observed functional alterations may serve as the mechanism by which WMHs contribute to poorer EF. Previous studies have suggested that WMHs may contribute to poor EF directly through disconnection of neural networks or indirectly through neurodegeneration secondary to vascular compromise (Brown et al., 2007; Debette and Markus, 2010). The latter is more consistent with our current results as WM microstructure did not predict baseline EF performance in the present study.

4.2. Longitudinal change in EF is predicted by baseline DMN and ECN WM microstructure

Our results indicated that baseline WM microstructure predicted longitudinal decline in EF over a three-year follow-up period. Previous results have shown that baseline WM microstructure (averaged across the entire brain) predicts longitudinal change in working memory (Charlton et al., 2010), and WM microstructure (averaged across several major tracts including the cingulum and corpus callosum) predicts fluid intelligence (Ritchie et al., 2015) over a period of years. In the current study, both microstructure within DMN WM pathways and within ECN WM pathways predicted longitudinal decline in EF in separate regression analyses.

Furthermore, results of linear mixed-modeling indicated that DMN and ECN WM microstructure appear to both independently and synergistically predict longitudinal change in EF. Together these results provide new evidence that WM microstructure within the ECN and DMN are strong predictors of longitudinal decline in performance on standardized neuropsychological tests of EF. These standardized neuropsychological EF tests are used as part of the diagnostic criteria for mild cognitive impairment (MCI) (Albert et al., 2011) and have been found to predict development of MCI and AD (Albert et al., 2001; Blacker et al., 2007; Gibbons et al., 2012). Therefore, with further refinement, the present DMN and ECN naWM templates may aid prediction of future cognitive decline and clinical diagnosis.

4.3. Longitudinal change in EF is predicted by AD pathology

The present study found that baseline CSF tau/Aβ_{42} ratios also predicted change in EF over the three-year follow-up period. A large body of work has focused on the use of AD markers to predict memory decline (Hedden et al., 2013), as well as prediction of clinical progression (Fagan et al., 2007; Vos et al., 2013). In contrast, less work has examined if AD pathology is predictive of EF performance declines. Several studies have demonstrated that increased AD pathology is associated with poorer EF performance cross-sectionally (Hedden et al., 2013; Oh et al., 2012), and one study demonstrated that higher CSF tau/Aβ_{42} ratios predict longitudinal decline in EF in CN older adults and those with MCI (van Harten et al., 2013). Our results are consistent with these findings in suggesting that baseline AD pathology impacts subsequent EF functioning.

4.4. DMN WM microstructure mediates the relationship between the tau/Aβ_{42} ratio and ΔEF

A key finding of the present study was that DMN WM microstructure mediated the relationship between the tau/Aβ_{42} ratio and ΔEF. Our mediation results provide the first evidence to our knowledge that AD pathology is associated with change in EF over time, in part, through its relationship with DMN WM microstructure. In addition, ECN WM microstructure partially mediated the relationship between the tau/Aβ_{42} ratio and ΔEF. This may represent the stronger association between AD pathology and the DMN at these early disease stages, and indicates the importance of WM microstructure in the AD pathological process. It is thus worth considering how Aβ_{42} and tau may negatively affect WM microstructure. Aβ_{42} has been show to disrupt myelin sheath formation and is toxic to oligodendrocytes responsible for maintenance and repair of myelin (Horiuchi et al., 2012; Lee et al., 2004; Xu et al., 2001). Further, abnormal aggregation of tau contributes to microtubule destabilization due to the loss of normal tau function (Alonso et al., 1994). Finally, tau

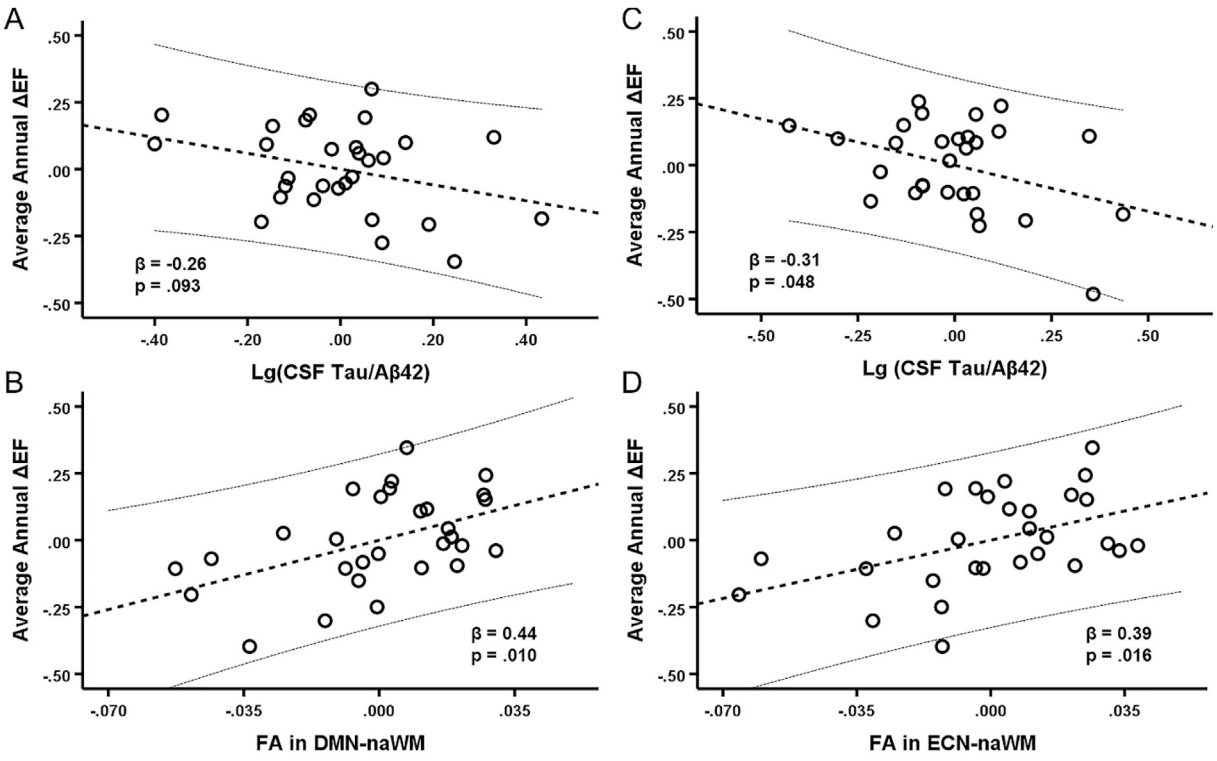

Fig. 5. Prediction of longitudinal ΔEF by baseline measures. A-B: Partial regression plots of average annual ΔEF against CSF tau/Aβ_{42} **(A)** and FA in DMN-naWM **(B)** simultaneously. **C-D:** Partial regression plots of average annual ΔEF against CSF tau/Aβ_{42} **(C)** and FA in ECN-naWM **(D)**. **A-D:** All values are demeaned. The thick dashed lines represent the linear best-fit and thin dashed lines are the 95% confidence intervals for the predicted response. Includes subset of participants included in longitudinal analyses (n = 29).

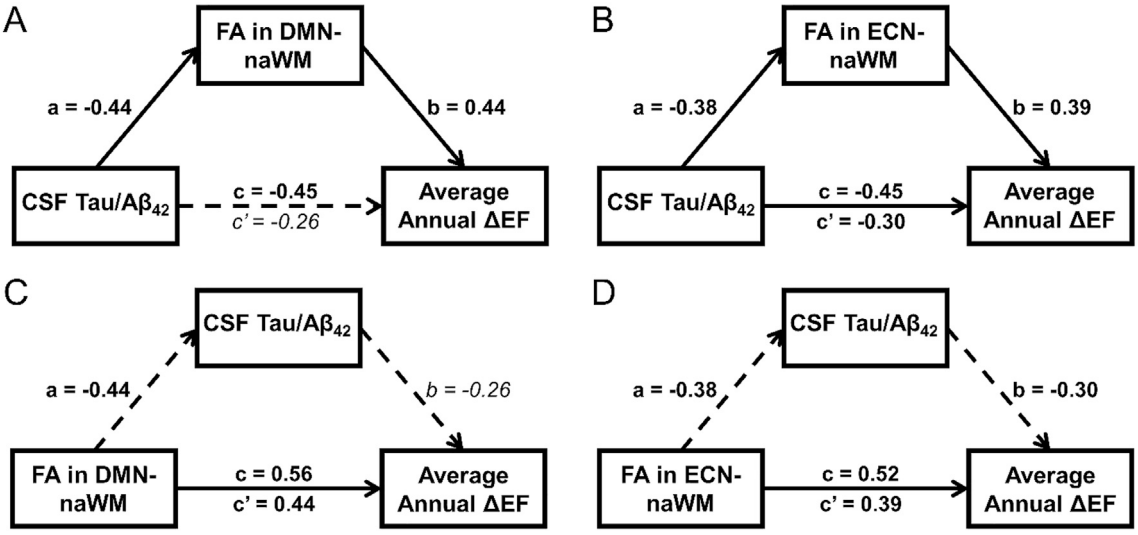

Fig. 6. Results of longitudinal mediation analyses. A-D: Results of Preacher and Hayes mediation analyses with significant direct or indirect effects indicated by solid arrows with non-significant direct or indirect effects are shown by dashed arrows. Standardized β-coefficients are shown next to the corresponding path with significant effects shown in bold and non-significant effects in italics. For all models, the total effect of X on Y (c) is shown above the horizontal arrow, while the direct effect of X on Y (c') after accounting for indirect effects is shown below the horizontal arrow. All models included the subset of participants used in longitudinal analyses (n = 29). **A:** Results indicated that the relationship between CSF Tau/Aβ_{42} ratio and average annual ΔEF was mediated by FA in DMN-naWM. **B:** Results indicated that the relationship between CSF Tau/Aβ_{42} ratio and average annual ΔEF was partially mediated by FA in ECN-naWM. **C-D:** Results indicated that CSF Tau/Aβ_{42} did not mediate the relationship between FA in DMN-naWM and average annual ΔEF **(C)** or the relationship between FA in ECN-naWM and ΔEF **(D)**.

and Aβ_{42} interact to disrupt fast axonal transport (FAT), which in turn contributes to decline in axonal, myelin, and synaptic integrity (Bartzokis, 2011; Vossel et al., 2015, 2010).

The direct effect of both DMN and ECN WM microstructure on change in EF suggests that additional, non-AD-related pathological changes in EF are also predicted by WM microstructure. Of relevance, we used FLAIR imaging to identify and mask out areas of WMH in order to study normal appearing WM (Brown et al., 2018). WMHs are ubiquitous in aging (de

Table 3
Linear mixed-modeling results.

Predictor	Model Fit	Year	Predictor	Predictor × Year
FA in DMN-naWM	AIC = 179.57	**$F_{1,78.9} = 9.97$ ($p = .002$)** **$\beta = -2.75$ [-4.50, -1.02]**	$F_{1,47.8} = 2.77$ ($p = .103$) $\beta = 6.75$ [-1.41, 14.91]	**$F_{1,78.9} = 9.27$ ($p = .003$)** **$\beta = 4.58$ [1.59, 7.57]**
DMN deactivation	AIC = 200.41	**$F_{1,78.4} = 7.64$ ($p = .007$)** **$\beta = -0.16$ [-0.28, -0.05]**	$F_{1,43.5} = 0.73$ ($p = .396$) $\beta = -0.16$ [-1.32, 3.28]	$F_{1,77.9} = 2.13$ ($p = .149$) $\beta = 0.54$ [-0.20, 1.27]
FA in ECN-naWM	AIC = 178.55	**$F_{1,78.9} = 13.83$ ($p < .001$)** **$\beta = -3.03$ [-4.66, -1.41]**	$F_{1,81.2} = 0.26$ ($p = .871$) $\beta = -0.76$ [-10.13, 8.60]	**$F_{1,79.0} = 12.96$ ($p = .001$)** **$\beta = 5.16$ [2.31, 8.01]**
ECN Activation	AIC = 203.89	$F_{1,78.9} = 5.14$ ($p = .026$) $\beta = -0.13$ [-0.23, −.02]	$F_{1,76.0} = 3.78$ ($p = .056$) $\beta = -1.35$ [-2.74, 0.03]	$F_{1,79.1} = 0.54$ ($p = .464$) $\beta = 0.15$ [-0.25, 0.54]
WMH Volume	AIC = 206.17	$F_{1,78.2} = 0.78$ ($p = .781$) $\beta = 0.16$ [-0.99, 1.32]	$F_{1,79.1} = 2.55$ ($p = .114$) $\beta = -0.34$ [-0.77, 0.08]	$F_{1,78.1} = 0.20$ ($p = .655$) $\beta = -0.03$ [−0.15, 0.09]
CSF tau/Aβ_{42}	AIC = 205.70	$F_{1,78.3} = 3.99$ ($p = .049$) $\beta = -0.29$ [-0.57, −0.001]	$F_{1,41.6} = 0.002$ ($p = .97$) $\beta = 0.27$ [-1.27, 1.30]	$F_{1,78.2} = 1.83$ ($p = .181$) $\beta = -0.27$ [-0.68, 0.13]

Results of separate linear mixed-models are shown in each row above. The model-fit is described by AIC, where lower values indicate a better fit. For each fixed-effect the fit statistic and un-standardized β co-efficient estimates are provided with the p-value and [95% CI], respectively. Significant effects with $p < .008$ are indicated in bold. All models included an intercept term.

Table 4
Linear Mixed Model Results using FA in DMN and FPCN naWM.

Predictor	Model 1 AIC = 164.65	Model 2 AIC = 137.49
Time	**$F_{1,78.0} = 12.40$** **($p = .001$)** **$\beta = -2.93$ [-4.58,-1.27]**	**$F_{1,77.9} = 5.50$** **($p = .022$)** **$\beta = -41.1$ [-76.0,-6.20]**
FA in DMN-naWM	$F_{1,46.8} = 3.09$ ($p = .085$) $\beta = 17.24$ [-2.49,36.97]	$F_{1,45.3} = 3.18$ ($p = .081$) $\beta = -149.2$ [-317.7,19.27]
FA in FPCN-naWM	$F_{1,47.3} = 1.28$ ($p = .263$) $\beta = -10.5$ [-29.2,8.16]	**$F_{1,45.4} = 4.55$** **($p = .038$)** **$\beta = -168.5$ [-327.7,-9.37]**
FA in DMN-naWM x Time	$F_{1,79.6} = 0.175$ ($p = .677$) $\beta = -1.56$ [-9.01,5.88]	**$F_{1,77.6} = 4.52$** **($p = .037$)** **$\beta = 68.2$** **[4.31,132.2]**
FA in FPCN-naWM x Time	$F_{1,80.1} = 3.072$ ($p = .083$) $\beta = 6.49$ [-0.88,13.86]	**$F_{1,78.2} = 5.60$** **($p = .020$)** **$\beta = 74.27$** **[11.78,136.8]**
FA in DMN-naWM x FA in FPCN-naWM	N/A	$F_{1,45.4} = 4.03$ ($p = .051$) $\beta = 292.0$ [-0.97,585.0]
FA in DMN-naWM x FA in FPCN-naWM x Time	N/A	**$F_{1,77.9} = 4.76$** **($p = .032$)** **$\beta = -123.6$ [-236.4,-10.83]**

Results of separate linear mixed-models are shown in each column above. The model-fit is described by AIC, where lower values indicate a better fit. For each fixed-effect the fit statistic and un-standardized β co-efficient estimates are provided with the p-value and [95% CI], respectively. Both models included an intercept term.

Leeuw, 2001) and are thought to primarily reflect areas of cerebrovascular pathology resulting from a breakdown in vascular integrity (Young et al., 2008). In contrast, declines in naWM are thought to reflect subtler declines in the microstructural organization of WM (van Norden et al., 2012). These changes may be the result of age-related declines in synapses, axonal loss, or myelin breakdown, all of which would reduce WM microstructure through loss of membrane density and organizational coherence (Bartzokis et al., 2004; Marner et al., 2003; Masliah et al., 1993; Tang et al., 1990). In addition, these changes may also reflect distal effects in tracts negatively impacted by cerebrovascular pathology (van Norden et al., 2012). Therefore, WM microstructure appears to be a sensitive marker that likely reflects a combination of age-related, AD pathology-related, and cerebrovascular pathology-related processes that each contribute to poorer EF outcomes.

4.5. Baseline and longitudinal EF are predicted by different functional/structural network measures

The DMN and ECN were found to be predictors of both baseline EF and ΔEF. However, baseline EF was only predicted by DMN and ECN functional patterns, while DMN and ECN WM microstructure were the most direct predictors of ΔEF. It is unclear what may cause this shift, but one possibility may be that functional brain measures reflect more dynamic processes that undergo greater day-to-day fluctuations and brain function may thus be a better predictor of more proximal EF performance. In contrast, measures of brain structure, which are often considered measures of 'brain reserve', likely show less fluctuation over short periods of time and would thus be expected to be more stable predictors of future cognitive performance than functional measures. While speculative, this possibility is generally in-line with a view that compensatory functional mechanisms become less effective in the context of increasing disruption of the structural network over time, thus aspects of brain reserve become more important (Barulli and Stern, 2013).

4.6. Limitations

The current study has several limitations. First, while baseline measures predicted ΔEF, causality cannot be directly inferred from the present results. For example, it is possible that some other unmeasured variable may be responsible for the observed relationships and mediation effects as these analyses are all hypothesis-driven correlational approaches. In addition, the present study had a limited sample size and may have been underpowered to detect smaller effects on EF cross-sectionally and longitudinally. Future work should use larger cohorts in order to better detect subtler effects. Further, we examine only CN older adults. It is unclear whether these relationships are maintained in states of mild cognitive impairment and clinical dementia. Future studies should seek to investigate the role of DMN WM and deactivation predicting EF in these later clinical stages. Finally, we treated AD pathology as a continuous variable, but it is unclear whether the relationship between AD pathology and other measures may be different above and below certain thresholds. Future studies should be performed with large enough samples to assess the effects of AD pathology on brain structure/function and EF both within sub- and supra-threshold groups and across all participants.

4.7. Conclusions

The current study provides evidence for relationships between multiple functional and structural factors in the DMN and ECN and EF performance on standardized neuropsychological measures. Further, our results provide novel evidence that baseline AD pathology negatively

impacts subsequent EF performance, in part, through its association with poorer WM microstructure within the DMN. Measures of WM microstructure may thus aid the monitoring and assessment of future therapeutic interventions aimed at preventing longitudinal EF declines.

Declarations of interest

None.

Acknowledgments

This study was supported by the National Institute on Aging and National Center for Advancing Translational Sciences of the National Institutes of Health (grant numbers R01AG033036, R01AG055449, P30AG028383, P01AG030128, TL1TR001997). The content is solely the responsibility of the authors and does not necessarily represent the official views of these granting agencies. The authors declare no competing financial interests. The authors thank, Dr. Gregory Jicha for performing some of the lumbar punctures, Drs. Jon Trojanowski and Leslie Shaw for CSF analysis, Beverly Meacham for conducting some of the MRI scans, and Drs. Erin Abner and Richard Kryscio for providing biostatistics consultation.

References

Albert, M.S., DeKosky, S.T., Dickson, D., Dubois, B., Feldman, H.H., Fox, N.C., Gamst, A., Holtzman, D.M., Jagust, W.J., Petersen, R.C., Snyder, P.J., Carrillo, M.C., Thies, B., Phelps, C.H., 2011. The diagnosis of mild cognitive impairment due to Alzheimer's disease: recommendations from the National Institute on Aging-Alzheimer's Association workgroups on diagnostic guidelines for Alzheimer's disease. Alzheimers. Dement. 7, 270–279. https://doi.org/10.1016/j.jalz.2011.03.008.

Albert, M.S., Moss, M.B., Tanzi, R., Jones, K., 2001. Preclinical prediction of AD using neuropsychological tests. J. Int. Neuropsychol. Soc. 7, 631–639.

Almkvist, O., 1996. Neuropsychological features of early Alzheimer's disease: preclinical and clinical stages. Acta Neurol. Scand. 94, 63–71. https://doi.org/10.1111/j.1600-0404.1996.tb05874.x.

Alonso, A.C., Zaidi, T., Grundke-Iqbal, I., Iqbal, K., 1994. Role of abnormally phosphorylated tau in the breakdown of microtubules in Alzheimer disease. Proc. Natl. Acad. Sci. U. S. A 91, 5562–5566.

Andersson, J.L.R., Graham, M.S., Zsoldos, E., Sotiropoulos, S.N., 2016. Incorporating outlier detection and replacement into a non-parametric framework for movement and distortion correction of diffusion MR images. Neuroimage 141, 556–572. https://doi.org/10.1016/j.neuroimage.2016.06.058.

Andersson, J.L.R., Sotiropoulos, S.N., 2016. An integrated approach to correction for off-resonance effects and subject movement in diffusion MR imaging. Neuroimage 125, 1063–1078. https://doi.org/10.1016/j.neuroimage.2015.10.019.

Andrews-Hanna, J.R., Smallwood, J., Spreng, R.N., 2014. The default network and self-generated thought: component processes, dynamic control, and clinical relevance. Ann. N. Y. Acad. Sci. 1316, 29–52. https://doi.org/10.1111/nyas.12360.

Bartzokis, G., 2011. Alzheimer's disease as homeostatic responses to age-related myelin breakdown. Neurobiol. Aging 32, 1341–1371. https://doi.org/10.1016/j.neurobiolaging.2009.08.007.

Bartzokis, G., Sultzer, D., Lu, P.H., Nuechterlein, K.H., Mintz, J., Cummings, J.L., 2004. Heterogeneous age-related breakdown of white matter structural integrity: implications for cortical "disconnection" in aging and Alzheimer's disease. Neurobiol. Aging 25, 843–851. https://doi.org/10.1016/j.neurobiolaging.2003.09.005.

Barulli, D., Stern, Y., 2013. Efficiency, capacity, compensation, maintenance, plasticity: emerging concepts in cognitive reserve. Trends Cognit. Sci. 17, 502–509. https://doi.org/10.1016/j.tics.2013.08.012.

Beaulieu, C., 2002. The basis of anisotropic water diffusion in the nervous system - a technical review. NMR Biomed. 15, 435–455. https://doi.org/10.1002/nbm.782.

Behrens, T.E.J., Berg, H.J., Jbabdi, S., Rushworth, M.F.S., Woolrich, M.W., 2007. Probabilistic diffusion tractography with multiple fibre orientations: what can we gain? Neuroimage 34, 144–155. https://doi.org/10.1016/j.neuroimage.2006.09.018.

Bell-McGinty, S., Podell, K., Franzen, M., Baird, A.D., Williams, M.J., 2002. Standard measures of executive function in predicting instrumental activities of daily living in older adults. Int. J. Geriatr. Psychiatry 17, 828–834. https://doi.org/10.1002/gps.646.

Blacker, D., Lee, H., Muzikansky, A., Martin, E.C., Tanzi, R., McArdle, J.J., Moss, M., Albert, M., 2007. Neuropsychological measures in normal individuals that predict subsequent cognitive decline. Arch. Neurol. 64, 862. https://doi.org/10.1001/archneur.64.6.862.

Breteler, M.M., van Swieten, J.C., Bots, M.L., Grobbee, D.E., Claus, J.J., van den Hout, J.H., van Harskamp, F., Tanghe, H.L., de Jong, P.T., van Gijn, J., 1994. Cerebral white matter lesions, vascular risk factors, and cognitive function in a population-based study: the Rotterdam Study. Neurology 44, 1246–1252. https://doi.org/10.1212/wnl.56.7.921.

Brown, C. a., Hakun, J.G., Zhu, Z., Johnson, N.F., Gold, B.T., 2015. White matter microstructure contributes to age-related declines in task-induced deactivation of the default mode network. Front. Aging Neurosci. 7 https://doi.org/10.3389/fnagi.2015.00194.

Brown, C.A., Jiang, Y., Smith, C.D., Gold, B.T., 2018. Age and Alzheimer's pathology disrupt default mode network functioning via alterations in white matter microstructure but not hyperintensities. Cortex. https://doi.org/10.1016/J.CORTEX.2018.04.006.

Brown, C.A., Johnson, N.F., Anderson-Mooney, A.J., Jicha, G.A., Shaw, L.M., Trojanowski, J.Q., Van Eldik, L.J., Schmitt, F.A., Smith, C.D., Gold, B.T., 2017. Development, validation and application of a new fornix template for studies of aging and preclinical Alzheimer's disease. NeuroImage Clin 13, 106–115. https://doi.org/10.1016/j.nicl.2016.11.024.

Brown, W.R., Moody, D.M., Thore, C.R., Challa, V.R., Anstrom, J.A., 2007. Vascular dementia in leukoaraiosis may be a consequence of capillary loss not only in the lesions, but in normal-appearing white matter and cortex as well. J. Neurol. Sci. 257, 62–66. https://doi.org/10.1016/j.jns.2007.01.015.

Buckner, R.L., Snyder, A.Z., Shannon, B.J., LaRossa, G., Sachs, R., Fotenos, A.F., Sheline, Y.I., Klunk, W.E., Mathis, C.A., Morris, J.C., Mintun, M.A., 2005. Molecular, structural, and functional characterization of Alzheimer's disease: evidence for a relationship between default activity, amyloid, and memory. J. Neurosci. 25, 7709–7717. https://doi.org/10.1523/JNEUROSCI.2177-05.2005.

Charlton, R.A., Schiavone, F., Barrick, T.R., Morris, R.G., Markus, H.S., 2010. Diffusion tensor imaging detects age related white matter change over a 2 year follow-up which is associated with working memory decline. J. Neurol. Neurosurg. Psychiatry 81, 13–19. https://doi.org/10.1136/jnnp.2008.167288.

COHEN, R.A., PAUL, R.H., OTT, B.R., MOSER, D.J., ZAWACKI, T.M., STONE, W., GORDON, N., 2002. The relationship of subcortical MRI hyperintensities and brain volume to cognitive function in vascular dementia. J. Int. Neuropsychol. Soc. 8 https://doi.org/10.1017/S1355617702860027. S1355617702860027.

Cole, M.W., Schneider, W., 2007. The cognitive control network: integrated cortical regions with dissociable functions. Neuroimage 37, 343–360. https://doi.org/10.1016/J.NEUROIMAGE.2007.03.071.

Crane, P.K., Narasimhalu, K., Gibbons, L.E., Pedraza, O., Mehta, K.M., Tang, Y., Manly, J.J., Reed, B.R., Mungas, D.M., 2008. Composite scores for executive function items: demographic heterogeneity and relationships with quantitative magnetic resonance imaging. J. Int. Neuropsychol. Soc. 14, 746–759. https://doi.org/10.1017/S1355617708081162.

Dale, A.M., Fischl, B., Sereno, M.I., 1999. Cortical surface-based analysis: I. Segmentation and surface reconstruction. Neuroimage 9, 179–194. https://doi.org/10.1006/nimg.1998.0395.

Daselaar, S.M., Iyengar, V., Davis, S.W., Eklund, K., Hayes, S.M., Cabeza, R.E., 2013. Less wiring, more firing: low-performing older adults compensate for impaired white matter with greater neural activity. Cerebr. Cortex. https://doi.org/10.1093/cercor/bht289 bht289.

de Leeuw, F.-E., 2001. Prevalence of cerebral white matter lesions in elderly people: a population based magnetic resonance imaging study. The Rotterdam Scan Study. J. Neurol. Neurosurg. Psychiatry 70, 9–14. https://doi.org/10.1136/jnnp.70.1.9.

Debette, S., Markus, H.S., 2010. The clinical importance of white matter hyperintensities on brain magnetic resonance imaging: systematic review and meta-analysis. BMJ 341, c3666. https://doi.org/10.1136/bmj.c3666.

Fagan, A.M., Roe, C.M., Xiong, C., Mintun, M.A., Morris, J.C., Holtzman, D.M., 2007. Cerebrospinal fluid tau/beta-amyloid(42) ratio as a prediction of cognitive decline in nondemented older adults. Arch. Neurol. 64, 343–349. https://doi.org/10.1001/archneur.64.3.noc60123.

Fischl, B., Salat, D.H., Busa, E., Albert, M., Dieterich, M., Haselgrove, C., van der Kouwe, A., Killiany, R., Kennedy, D., Klaveness, S., Montillo, A., Makris, N., Rosen, B., Dale, A.M., 2002. Whole brain segmentation: automated labeling of neuroanatomical structures in the human brain. Neuron 33, 341–355. https://doi.org/10.1016/S0896-6273(02)00569-X.

Gibbons, L.E., Carle, A.C., Mackin, R.S., Harvey, D., Mukherjee, S., Insel, P., Curtis, S.M., Mungas, D., Crane, P.K., 2012. A composite score for executive functioning, validated in Alzheimer's Disease Neuroimaging Initiative (ADNI) participants with baseline mild cognitive impairment. Brain Imaging Behav 6, 517–527. https://doi.org/10.1007/s11682-012-9176-1.

Glenner, G.G., Wong, C.W., 1984. Alzheimer's disease: Initial report of the purification and characterization of a novel cerebrovascular amyloid protein. Biochem. Biophys. Res. Commun. 120, 885–890. https://doi.org/10.1016/S0006-291X(84)80190-4.

Gold, B.T., Brown, C.A., Hakun, J.G., Shaw, L.M., Trojanowski, J.Q., Smith, C.D., 2017. Clinically silent Alzheimer's and vascular pathologies influence brain networks supporting executive function in healthy older adults. Neurobiol. Aging 58, 102–111. https://doi.org/10.1016/J.NEUROBIOLAGING.2017.06.012.

Gold, B.T., Powell, D.K., Xuan, L., Jicha, G.A., Smith, C.D., 2010. Age-related slowing of task switching is associated with decreased integrity of frontoparietal white matter. Neurobiol. Aging 31, 512–522. https://doi.org/10.1016/j.neurobiolaging.2008.04.005.

Gold, B.T., Zhu, Z., Brown, C.A., Andersen, A.H., LaDu, M.J., Tai, L., Jicha, G.A., Kryscio, R.J., Estus, S., Nelson, P.T., Scheff, S.W., Abner, E., Schmitt, F.A., Van Eldik, L.J., Smith, C.D., 2014. White matter integrity is associated with cerebrospinal fluid markers of Alzheimer's disease in normal adults. Neurobiol. Aging 35, 2263–2271. https://doi.org/10.1016/j.neurobiolaging.2014.04.030.

Gould, R.L., Brown, R.G., Owen, A.M., Bullmore, E.T., Howard, R.J., 2006. Task-induced deactivations during successful paired associates learning: an effect of age but not Alzheimer's disease. Neuroimage 31, 818–831. https://doi.org/10.1016/j.neuroimage.2005.12.045.

Grady, C., 2012. The cognitive neuroscience of ageing. Nat. Rev. Neurosci. 13, 491–505. https://doi.org/10.1038/nrn3256.
Grady, C.L., Springer, M.V., Hongwanishkul, D., McIntosh, A.R., Winocur, G., 2006. Age-related changes in brain activity across the adult lifespan. J. Cogn. Neurosci. 18, 227–241. https://doi.org/10.1162/089892906775783705.
Grafton, S.T., Sumi, S.M., Stimac, G.K., Alvord, E.C., Shaw, C.M., Nochlin, D., 1991. Comparison of postmortem magnetic resonance imaging and neuropathologic findings in the cerebral white matter. Arch. Neurol. 48, 293–298.
Grundke-Iqbal, I., Iqbal, K., Tung, Y.C., Quinlan, M., Wisniewski, H.M., Binder, L.I., 1986. Abnormal phosphorylation of the microtubule-associated protein tau (tau) in Alzheimer cytoskeletal pathology. Proc. Natl. Acad. Sci. 83, 4913–4917. https://doi.org/10.1073/pnas.83.13.4913.
Hayes, A.F., 2013. An Introduction to Mediation, Moderation, and Conditional Process Analysis: A Regression-Based Approach, third ed. Guilford Press, New York, NY.
Hedden, T., Oh, H., Younger, A.P., Patel, T.A., 2013. Meta-analysis of amyloid-cognition relations in cognitively normal older adults. Neurology 80, 1341–1348. https://doi.org/10.1212/WNL.0b013e31828ab35d.
Hedden, T., Van Dijk, K.R.A., Shire, E.H., Sperling, R.A., Johnson, K.A., Buckner, R.L., 2012. Failure to modulate attentional control in advanced aging linked to white matter pathology. Cerebr. Cortex 22, 1038–1051. https://doi.org/10.1093/cercor/bhr172.
Horiuchi, M., Maezawa, I., Itoh, A., Wakayama, K., Jin, L.W., Itoh, T., DeCarli, C., 2012. Amyloid ??1-42 oligomer inhibits myelin sheet formation in vitro. Neurobiol. Aging 33, 499–509. https://doi.org/10.1016/j.neurobiolaging.2010.05.007.
Jenkinson, M., Beckmann, C.F., Behrens, T.E.J., Woolrich, M.W., Smith, S.M., 2012. FSL. Neuroimage 62, 782–790. https://doi.org/10.1016/j.neuroimage.2011.09.015.
Jiang, Y., 2000. Complementary neural mechanisms for tracking items in human working memory. Science (80-.) 287, 643–646. https://doi.org/10.1126/science.287.5453.643.
Kane, M.J., Engle, R.W., 2002. The role of prefrontal cortex in working-memory capacity, executive attention, and general fluid intelligence: an individual-differences perspective. Psychon. Bull. Rev. 9, 637–671. https://doi.org/10.3758/BF03196323.
Kantarci, K., Schwarz, C.G., Reid, R.I., Przybelski, S.A., Lesnick, T.G., Zuk, S.M., Senjem, M.L., Gunter, J.L., Lowe, V., Machulda, M.M., Knopman, D.S., Petersen, R.C., Jack, C.R., 2014. White matter integrity determined with diffusion tensor imaging in older adults without dementia: influence of amyloid load and neurodegeneration. JAMA Neurol 71, 1547–1554. https://doi.org/10.1001/jamaneurol.2014.1482.
Kryscio, R.J., Abner, E.L., Jicha, G.A., Nelson, P.T., Smith, C.D., Van Eldik, L.J., Lou, W., Fardo, D.W., Cooper, G.E., Schmitt, F.A., 2016. Self-reported memory complaints: a comparison of demented and unimpaired outcomes. J. Prev. Alzheimer's Dis.
Lee, J.T., Xu, J., Lee, J.M., Ku, G., Han, X., Yang, D.I., Chen, S., Hsu, C.Y., 2004. Amyloid-?? peptide induces oligodendrocyte death by activating the neutral sphingomyelinase-ceramide pathway. J. Cell Biol. 164, 123–131. https://doi.org/10.1083/jcb.200307017.
Lustig, C., Snyder, A.Z., Bhakta, M., O'Brien, K.C., McAvoy, M., Raichle, M.E., Morris, J.C., Buckner, R.L., 2003. Functional deactivations: change with age and dementia of the Alzheimer type. Proc. Natl. Acad. Sci. U. S. A 100, 14504–14509. https://doi.org/10.1073/pnas.2235925100.
Madden, D.J., Whiting, W.L., Huettel, S.A., White, L.E., MacFall, J.R., Provenzale, J.M., 2004. Diffusion tensor imaging of adult age differences in cerebral white matter: relation to response time. Neuroimage 21, 1174–1181. https://doi.org/10.1016/j.neuroimage.2003.11.004.
Marner, L., Nyengaard, J.R., Tang, Y., Pakkenberg, B., 2003. Marked loss of myelinated nerve fibers in the human brain with age. J. Comp. Neurol. 462, 144–152. https://doi.org/10.1002/cne.10714.
Masliah, E., Mallory, M., Hansen, L., DeTeresa, R., Terry, R.D., 1993. Quantitative synaptic alterations in the human neocortex during normal aging. Neurology 43. https://doi.org/10.1212/WNL.43.1_Part_1.192, 192–192.
Miller, E.K., Cohen, J.D., 2001. An integrative theory of prefrontal cortex function. Annu. Rev. Neurosci. 24, 167–202. https://doi.org/10.1146/annurev.neuro.24.1.167.
Morris, J.C., Storandt, M., McKeel, D.W., Rubin, E.H., Price, J.L., Grant, E.A., Berg, L., 1996. Cerebral amyloid deposition and diffuse plaques in "normal" aging: Evidence for presymptomatic and very mild Alzheimer's disease. Neurology 46, 707–719. https://doi.org/10.1212/WNL.46.3.707.
Niendam, T.A., Laird, A.R., Ray, K.L., Dean, Y.M., Glahn, D.C., Carter, C.S., 2012. Meta-analytic evidence for a superordinate cognitive control network subserving diverse executive functions. Cognit. Affect Behav. Neurosci. 12, 241–268. https://doi.org/10.3758/s13415-011-0083-5.
Oh, H., Madison, C., Haight, T.J., Markley, C., Jagust, W.J., 2012. Effects of age and β-amyloid on cognitive changes in normal elderly people. Neurobiol. Aging 33, 2746–2755. https://doi.org/10.1016/j.neurobiolaging.2012.02.008.
Oh, H., Steffener, J., Razlighi, Q.R., Habeck, C., Liu, D., Gazes, Y., Janicki, S., Stern, Y., 2015. Aβ-related hyperactivation in frontoparietal control regions in cognitively normal elderly. Neurobiol. Aging 36, 3247–3254. https://doi.org/10.1016/j.neurobiolaging.2015.08.016.
Park, D.C., Reuter-Lorenz, P., 2009. The adaptive brain: aging and neurocognitive scaffolding. Annu. Rev. Psychol. 60, 173–196. https://doi.org/10.1146/annurev.psych.59.103006.093656.
Pathy, M.S.J., Sinclair, A.J., Morley, J.E., 2006. Principles and Practice of Geriatric Medicine. John Wiley & Sons.
Persson, J., Lustig, C., Nelson, J.K., Reuter-Lorenz, P.A., 2007. Age differences in deactivation: a link to cognitive control? J. Cogn. Neurosci. 19, 1021–1032. https://doi.org/10.1162/jocn.2007.19.6.1021.
Power, J.D., Barnes, K.A., Snyder, A.Z., Schlaggar, B.L., Petersen, S.E., 2012. Spurious but systematic correlations in functional connectivity MRI networks arise from subject motion. Neuroimage 59, 2142–2154. https://doi.org/10.1016/j.neuroimage.2011.10.018.
Prakash, R.S., Heo, S., Voss, M.W., Patterson, B., Kramer, A.F., 2012. Age-related differences in cortical recruitment and suppression: implications for cognitive performance. Behav. Brain Res. 230, 192–200. https://doi.org/10.1016/j.bbr.2012.01.058.
Price, J.L., McKeel, D.W., Buckles, V.D., Roe, C.M., Xiong, C., Grundman, M., Hansen, L.A., Petersen, R.C., Parisi, J.E., Dickson, D.W., Smith, C.D., Davis, D.G., Schmitt, F.A., Markesbery, W.R., Kaye, J., Kurlan, R., Hulette, C., Kurland, B.F., Higdon, R., Kukull, W., Morris, J.C., 2009. Neuropathology of nondemented aging: presumptive evidence for preclinical Alzheimer disease. Neurobiol. Aging 30, 1026–1036. https://doi.org/10.1016/j.neurobiolaging.2009.04.002.
Raichle, M.E., MacLeod, A.M., Snyder, A.Z., Powers, W.J., Gusnard, D.A., Shulman, G.L., 2001. A default mode of brain function. Proc. Natl. Acad. Sci. U. S. A. 98, 676–682. https://doi.org/10.1073/pnas.98.2.676.
Ritchie, S.J., Bastin, M.E., Tucker-Drob, E.M., Maniega, S.M., Engelhardt, L.E., Cox, S.R., Royle, N.A., Gow, A.J., Corley, J., Pattie, A., Taylor, A.M., Valdes Hernandez, M., del, C., Starr, J.M., Wardlaw, J.M., Deary, I.J., 2015. Coupled changes in brain white matter microstructure and fluid intelligence in later life. J. Neurosci. 35, 8672–8682. https://doi.org/10.1523/JNEUROSCI.0862-15.2015.
Rypma, B., Berger, J.S., Prabhakaran, V., Bly, B.M., Kimberg, D.Y., Biswal, B.B., D'Esposito, M., 2006. Neural correlates of cognitive efficiency. Neuroimage 33, 969–979. https://doi.org/10.1016/j.neuroimage.2006.05.065.
Salat, D.H., Tuch, D.S., Greve, D.N., van der Kouwe, a J.W., Hevelone, N.D., Zaleta, a K., Rosen, B.R., Fischl, B., Corkin, S., Rosas, H.D., Dale, a M., 2005. Age-related alterations in white matter microstructure measured by diffusion tensor imaging. Neurobiol. Aging 26, 1215–1227. https://doi.org/10.1016/j.neurobiolaging.2004.09.017.
Salthouse, T.A., 2011. What cognitive abilities are involved in trail-making performance? Intelligence 39, 222–232. https://doi.org/10.1016/j.intell.2011.03.001.
Schmitt, F.A., Nelson, P.T., Abner, E., Scheff, S., Jicha, G.A., Smith, C., Cooper, G., Mendiondo, M., Danner, D.D., Van Eldik, L.J., Caban-Holt, A., Lovell, M.A., Kryscio, R.J., 2012. University of Kentucky Sanders-Brown healthy brain aging volunteers: donor characteristics, procedures and neuropathology. Curr. Alzheimer Res. 9, 724–733.
Shaw, L.M., Vanderstichele, H., Knapik-Czajka, M., Clark, C.M., Aisen, P.S., Petersen, R.C., Blennow, K., Soares, H., Simon, A., Lewczuk, P., Dean, R., Siemers, E., Potter, W., Lee, V.M.-Y., Trojanowski, J.Q., 2009. Cerebrospinal fluid biomarker signature in Alzheimer's disease neuroimaging initiative subjects. Ann. Neurol. 65, 403–413. https://doi.org/10.1002/ana.21610.
Smith, C.D., Johnson, E.S., Van Eldik, L.J., Jicha, G.A., Schmitt, F.A., Nelson, P.T., Kryscio, R.J., Murphy, R.R., Wellnitz, C.V., 2016. Peripheral (deep) but not periventricular MRI white matter hyperintensities are increased in clinical vascular dementia compared to Alzheimer's disease. Brain Behav 6, e00438. https://doi.org/10.1002/brb3.438.
Smith, S.M., Jenkinson, M., Johansen-Berg, H., Rueckert, D., Nichols, T.E., Mackay, C.E., Watkins, K.E., Ciccarelli, O., Cader, M.Z., Matthews, P.M., Behrens, T.E.J., 2006. Tract-based spatial statistics: voxelwise analysis of multi-subject diffusion data. Neuroimage 31, 1487–1505. https://doi.org/10.1016/j.neuroimage.2006.02.024.
Smith, S.M., Jenkinson, M., Woolrich, M.W., Beckmann, C.F., Behrens, T.E.J., Johansen-Berg, H., Bannister, P.R., De Luca, M., Drobnjak, I., Flitney, D.E., Niazy, R.K., Saunders, J., Vickers, J., Zhang, Y., De Stefano, N., Brady, J.M., Matthews, P.M., 2004. Advances in functional and structural MR image analysis and implementation as FSL. Neuroimage 23 (Suppl. 1), S208–S219. https://doi.org/10.1016/j.neuroimage.2004.07.051.
Sperling, R.A., Laviolette, P.S., O'Keefe, K., O'Brien, J., Rentz, D.M., Pihlajamaki, M., Marshall, G., Hyman, B.T., Selkoe, D.J., Hedden, T., Buckner, R.L., Becker, J.A., Johnson, K.A., 2009. Amyloid deposition is associated with impaired default network function in older persons without dementia. Neuron 63, 178–188. https://doi.org/10.1016/j.neuron.2009.07.003.
Spreng, R.N., Wojtowicz, M., Grady, C.L., 2010. Reliable differences in brain activity between young and old adults: a quantitative meta-analysis across multiple cognitive domains. Neurosci. Biobehav. Rev. 34, 1178–1194. https://doi.org/10.1016/j.neubiorev.2010.01.009.
Stern, Y., 2009. Cognitive reserve. Neuropsychologia 47, 2015–2028. https://doi.org/10.1016/j.neuropsychologia.2009.03.004.
Tang, Y., Nyengaard, J.R., Pakkenberg, B., Gundersen, H.J., Schweizer, A., de Groot, J., 1990. Age-induced white matter changes in the human brain: a stereological investigation. Neurobiol. Aging 18, 609–615. https://doi.org/10.1016/S0197-4580(97)00155-3.
Taylor, W.D., Bae, J.N., MacFall, J.R., Payne, M.E., Provenzale, J.M., Steffens, D.C., Krishnan, K.R.R., 2007. Widespread effects of hyperintense lesions on cerebral white matter structure. Am. J. Roentgenol. 188, 1695–1704. https://doi.org/10.2214/AJR.06.1163.
van Harten, A.C., Smits, L.L., Teunissen, C.E., Visser, P.J., Koene, T., Blankenstein, M.A., Scheltens, P., van der Flier, W.M., 2013. Preclinical AD predicts decline in memory and executive functions in subjective complaints. Neurology 81, 1409–1416. https://doi.org/10.1212/WNL.0b013e3182a8418b.
van Norden, A.G.W., de Laat, K.F., van Dijk, E.J., van Uden, I.W.M., van Oudheusden, L.J.B., Gons, R.A.R., Norris, D.G., Zwiers, M.P., de Leeuw, F.-E., 2012. Diffusion tensor imaging and cognition in cerebral small vessel disease. Biochim. Biophys. Acta (BBA) - Mol. Basis Dis. 1822, 401–407. https://doi.org/10.1016/j.bbadis.2011.04.008.
Vannini, P., Hedden, T., Becker, J.A., Sullivan, C., Putcha, D., Rentz, D., Johnson, K.A., Sperling, R.A., 2012. Age and amyloid-related alterations in default network

habituation to stimulus repetition. Neurobiol. Aging 33, 1237–1252. https://doi.org/10.1016/j.neurobiolaging.2011.01.003.

Vos, S.J., Xiong, C., Visser, P.J., Jasielec, M.S., Hassenstab, J., Grant, E.A., Cairns, N.J., Morris, J.C., Holtzman, D.M., Fagan, A.M., 2013. Preclinical Alzheimer's disease and its outcome: a longitudinal cohort study. Lancet Neurol. 12, 957–965. https://doi.org/10.1016/S1474-4422(13)70194-7.

Vossel, K.A., Xu, J.C., Fomenko, V., Miyamoto, T., Suberbielle, E., Knox, J.A., Ho, K., Kim, D.H., Yu, G.Q., Mucke, L., 2015. Tau reduction prevents Aβ-induced axonal transport deficits by blocking activation of GSK3β. J. Cell Biol. 209, 419–433. https://doi.org/10.1083/jcb.201407065.

Vossel, K.A., Zhang, K., Brodbeck, J., Daub, A.C., Sharma, P., Finkbeiner, S., Cui, B., Mucke, L., 2010. Tau reduction prevents Abeta-induced defects in axonal transport. Science (80-.) 330, 198. https://doi.org/10.1126/science.1194653.

Weintraub, S., Salmon, D., Mercaldo, N., Ferris, S., Graff-Radford, N.R., Chui, H., Cummings, J., DeCarli, C., Foster, N.L., Galasko, D., Peskind, E., Dietrich, W., Beekly, D.L., Kukull, W.A., Morris, J.C., 2002. The Alzheimer's disease centers' uniform data set (UDS): the neuropsychologic test battery. Alzheimers Dis. Assoc. Disord. 23, 91–101. https://doi.org/10.1097/WAD.0b013e318191c7dd.

Xu, J., Chen, S., Ahmed, S.H., Chen, H., Ku, G., Goldberg, M.P., Hsu, C.Y., 2001. Amyloid-beta peptides are cytotoxic to oligodendrocytes. J. Neurosci. 21, RC118.

Young, V.G., Halliday, G.M., Kril, J.J., 2008. Neuropathologic correlates of white matter hyperintensities. Neurology 71, 804–811. https://doi.org/10.1212/01.wnl.0000319691.50117.54.

Zelazo, P.D., Craik, F.I.M., Booth, L., 2004. Executive function across the life span. Acta Psychol. (Amst) 115, 167–183. https://doi.org/10.1016/j.actpsy.2003.12.005.

Zhu, Z., Johnson, N.F., Kim, C., Gold, B.T., 2015. Reduced frontal cortex efficiency is associated with lower white matter integrity in aging. Cerebr. Cortex 25, 138–146. https://doi.org/10.1093/cercor/bht212.